Unoccupied electronic states of the Cs/Cu(100) and Cs/Cu(111) adsorption systems

D. A. Arena, F. G. Curti, and R. A. Bartynski*
Department of Physics and Astronomy and Laboratory for Surface Modification, Rutgers University, P.O. Box 849, Piscataway, New Jersey 08855-0849
(Received 16 May 1997; revised manuscript received 15 September 1997)

We have investigated the unoccupied electronic structure of submonolayer amounts of cesium on the Cu(100) and Cu(111) surfaces by inverse photoemission (IPE) and work-function measurements. At very low Cs coverages on both substrates, IPE spectra obtained at normal incidence indicate that an adsorbate-induced feature develops in the projected bulk band gap of the substrate at an energy of ~ 3 eV above the Fermi level (E_F). As the Cs coverage is increased, this feature moves to lower energy. On the Cu(100) surface, the energy of the Cs feature initially follows the decrease of the work function, and levels off at ~ 0.3 eV above E_F as the Cs coverage approaches 1 ML. We observed a similar effect for the Cs/Cu(111) system. Off-normal spectra obtained for 0.08 ML of Cs on Cu(111) indicate that, at low coverages, the Cs state does not disperse with $k_{\|}$. However, on both substrates, we observed a correlation between modulations in the intensity of the Cs feature and degeneracy between this feature and the projected bulk bands of the substrate. Energy-dependent IPE spectra suggest that the adsorbate state on both Cu surfaces has predominantly d-like orbital character when the state is in the projected bulk band gap of the substrate. The orbital character of the Cs feature changes to sp-like when the adsorbate state is degenerate with the Cu sp-derived bulk bands. This effect was observed whether the degeneracy was achieved by varying the Cs coverage at a fixed $k_{\|}$, or by varying $k_{\|}$ at a fixed coverage. We interpret this as evidence of momentum-dependent hybridization of the adsorbate-substrate bond. [S0163-1829(97)03248-7]

I. INTRODUCTION

The bonding of alkali metals to simple and noble-metal surfaces was long considered to be a simple model of metal on metal adsorption. During the past ~ 15 years, however, experimental evidence coupled with renewed and sophisticated theoretical activity in the field has demonstrated that alkali-on-metal systems are far more complex than had been thought.[1–10] Indeed, the field has recently generated considerable controversy with ongoing debates over issues such as the degree of ionicity versus covalency in the alkali-metal substrate bond,[2–6] as well as the relative stability of substitutional versus on-top adsorption sites.[7–9] The surface structure of these systems has also proven to be more complex than anticipated, with many alkali-on-metal systems exhibiting a rich series of surface structures over a wide range of temperatures throughout the submonolayer coverage regime.[10]

With regard to electronic structure, much of the experimental effort to date has concentrated on the occupied electronic states of the lighter alkalis Li, Na, and K.[11–13] Furthermore, a large portion of the theoretical work has been limited to either complete monolayers or ordered structures that are encountered at relatively high coverages.[4,7,14–16] However, these factors are of limited use in understanding the initial adsorption properties of the heavier alkalis on metal surfaces. First, ordered overlayers do not typically form in the initial stages of adsorption, particularly for the alkali metals, where a dipole-dipole repulsion inhibits island formation.[17] Second, for the lighter alkalis, the occupied electronic structure consists primarily of relatively simple, singly occupied s orbital levels, while the unoccupied density of states near the Fermi level (E_F) for adsorbed layers is derived primarily from p orbitals.[18] In contrast, the unoccupied electronic states of the heavier alkalis include a significant contribution from a high density of d orbitals that are within a few eV of the Fermi level,[18] and play a critical role in bonding. Although the unoccupied electronic structure of some alkali-on-metal systems has been examined by inverse photoemission (IPE) studies, these efforts have been largely limited to isochromat spectroscopy of the lighter alkalis.[11,13,19–27] IPE investigations of Cs, in particular on metal surfaces, have been limited to isochromat spectroscopy of multilayer films,[28] ordered overlayers,[11] and at normal incidence.[13]

In this paper, we present an IPE study of Cs adsorption on the Cu(100) and Cu(111) surfaces. IPE spectra of the unoccupied electronic levels were acquired using an angle-resolved, photon-energy dispersive spectrograph. On both surfaces, a Cs-induced feature, assigned to the unoccupied Cs $5d$ level, is observed ~ 3 eV above the Fermi level at low coverages. Similar to the unoccupied p levels of other alkali adsorption systems, this feature disperses toward E_F as the coverage increases. However, spectra obtained at various excitation energies suggest that the orbital character of the Cs-induced feature depends on whether the state is degenerate with a substrate bulk band or whether it lies in a projected bulk band gap. This observation is interpreted in terms of an adsorbate-substrate coupling model developed by Liebsch.

This paper is organized as follows. Section II provides details on our UV spectrograph, and also describes our sample preparation techniques. Section III presents IPE spectra from Cs on Cu(100) as a function of adsorbate coverage, while Sec. IV discusses similar results for the Cs on Cu(111) system. In Sec. V we examine the excitation energy dependence of a subset of spectra presented in Secs. III and IV, where the intensity of the Cs-induced feature undergoes sig-

nificant changes in a narrow coverage range. We discuss and interpret our results in Sec. VI, and conclude and summarize our findings in Sec. VII.

II. EXPERIMENT

We acquired inverse photoemission spectra using a photon energy dispersive spectrograph that is described in detail elsewhere.[29] The major components of the system are a custom-built electron gun based on the Pierce-Stoffel design,[30] a concave spherical diffraction grating, and a movable two-dimensional position sensitive photon detector. All optical elements (sample, grating, and detector) are configured in a Rowland circle mounting for optimal focus. As a photon detector, we employ a Csl-coated multichannel plate mounted on an assembly which moves along an arc of the Rowland circle to increase the accessible energy range. The diffraction grating, which is ruled at 1200 lines per mm, has an opening angle between the incident radiation from the sample and the detector axis of 45°, and an entrance angle of 25° between the sample and the grating normal. The angle between the electron gun and the grating is fixed at 45°, and the electron angle of incidence on the sample is varied by rotating the sample about an axis perpendicular to its normal. The spectrograph as a whole is optimized for detection of photons in the 10 eV$\lesssim\hbar\omega\lesssim$40 eV range. The instrument has an optical resolving power of $E/\Delta E=70$, resulting in a total resolution of $\sim$0.3 eV at a photon energy of 20 eV. The spectrograph is attached to an ultrahigh-vacuum analytical chamber (base pressure of $\sim 8\times 10^{-11}$ torr) that houses the IPE electron gun, the sample, and a rear view low-energy electron-diffraction (LEED) system. Work-function measurements were performed in a retarding mode by measuring the stopping potential for current to the sample from the IPE electron gun.

The substrates in this study were Cu(100) and Cu(111) single-crystal surfaces. Each sample was mechanically polished to within 0.25° of the desired high-symmetry crystal face. An electrochemical etch was the final polishing step, and the samples were then introduced into the analysis chamber. Atomically clean, well-ordered surfaces were produced by several cycles of Ar^+-ion bombardment ($\sim$1 keV) followed by a $\sim$20-min anneal at 420 °C. Samples prepared in this fashion consistently produced sharp (1×1) LEED patterns. We verified the sample cleanliness by examining the normal-incidence inverse photoemission spectra of the surfaces. The image potential states of our samples, which are highly sensitive to surface contamination, were uniformly sharp, intense and occurred at the energies corresponding to clean surfaces.[31]

The Cs sources were commercial alkali getters, which were used to thermally deposit submonolayer amounts of Cs on the samples. We monitored the Cs coverages primarily by measuring the change in the work function of the sample during deposition.[17] This was cross checked using LEED, where a sharp quasihexagonal pattern on the Cu(100) and Cu(111) substrates was observed for full monolayer coverage at room temperatures.[32] In this paper, 1 ML refers to saturation coverage at room temperature, which corresponds to 4.12×10^{14} Cs atoms/cm^2 for Cu(100),[17] and 4.42×10^{14} Cs atoms/cm^2 for Cu(111).[33] Spectra from the Cu(100) sample were acquired at room temperature. The Cu(111) sample was in contact with a copper braid attached to a liquid-nitrogen reservoir for sample cooling. This arrangement allowed the Cu(111) sample to be cooled to $\sim$140 K during deposition and data acquisition. We observed a slight degradation of the IPE spectra after 30 min of data acquisition, and therefore limited our spectrum acquisition times to 20 min. Typically, several individually acquired spectra were combined to obtain the results presented in subsequent sections.

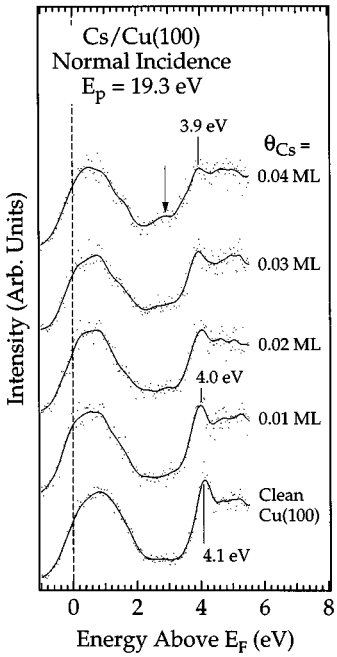

FIG. 1. Room-temperature, normal-incidence IPE spectra for very low coverages of Cs on Cu(100) obtained with an incident electron energy of 19.3 eV. The bottom spectrum is from clean Cu(100). Note the shift in the image potential state [feature at 4.1 eV above E_F on clean Cu(100)] with increasing Cs coverage. In the $\theta_{Cs}=0.04$ ML spectrum, the arrow identifies an adsorbate-induced feature which appears at 2.9 eV.

III. Cs ON Cu(100)

The results discussed in this section are based on room-temperature spectra acquired at normal incidence, i.e., at the Γ point of the surface Brillouin zone (SBZ), and at a constant incident electron energy of 19.3 eV. Figure 1 presents IPE spectra for very low coverages of Cs on Cu(100), with a clean Cu(100) spectrum at the bottom and increasing Cs coverages toward the top of the graph. The clean Cu(100) spectrum is dominated by two features: (1) strong emission from zero to 2 eV above E_F, originating from bulk direct transitions[34,35] and a surface resonance at $\sim$2 eV,[36,37] and (2) the sharp $n=1$ image potential state at about 4.1 eV above E_F.[31,37–39] The low-intensity region between these two features corresponds to the Cu band gap at the X point of the bulk Brillouin zone, projected onto the (100) surface.

The presence of even small amounts of Cs on this surface produces significant changes in the IPE spectrum. First, as Cs is deposited on the Cu, the intensity of the image potential state diminishes dramatically, which is an effect in cor-

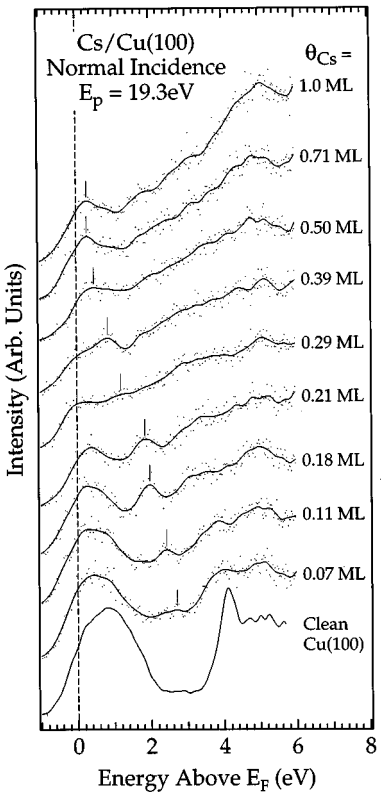

FIG. 2. Room-temperature, normal-incidence IPE spectra as a function of increasing Cs coverage on Cu(100). The incident electron energy is 19.3 eV. The bottom spectrum is from clean Cu(100). The Cs-induced state is indicated by the tick mark. Note the weakening of the adsorbate feature at $\theta_{Cs}=0.29$ ML.

respondence with the extreme sensitivity of this state to the presence of surface contaminants. In addition, the energy of the image potential state shifts subtly to lower energy. As the energy of image potential states on metals closely follows the vacuum level, this behavior is in line with the well-established decrease in the work function of alkali-covered metal surfaces.[1] By a coverage of $\theta_{Cs}=0.04$ ML, the energy of the image potential state has dropped by ~ 0.2 eV while, within experimental uncertainty, the work function has decreased by the same amount. At this point, the intensity of the Cu image state is considerably weaker than the corresponding feature on the clean Cu(100) spectrum. Moreover, at this coverage an additional spectral feature is visible in the region of the projected band gap of the substrate at an energy of ~ 2.9 eV above E_F. Although this feature is weak relative to the Cu peaks, it is distinct, reproducible, and well separated from both the Cu image potential state and the lower-energy bulk-related emission. We therefore conclude that the feature at ~ 2.9 eV is a spectral feature due to the presence of the adsorbate. As shall be discussed in Sec. V, the behavior of this feature is consistent with a state having significant d-like orbital character, and this feature is associated with the unoccupied Cs $5d$ level.

Figure 2 presents additional IPE spectra of the Cs/Cu(100) system as the Cs coverage is increased further. Again the bottom spectrum was obtained from clean Cu(100). At a coverage of $\theta_{Cs}=0.07$ ML, the weak remnant of the Cu image potential state is apparent at about 3.8 eV.

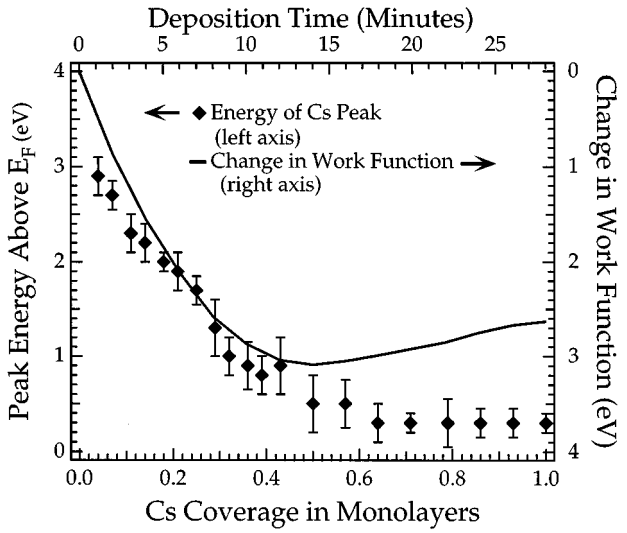

FIG. 3. Change in work function (right axis) and energies of the Cs feature (left axis) as a function of Cs coverage on Cu(100).

More importantly, a weak adsorbate-induced feature is again visible in the Cu-projected band gap. This peak is the same adsorbate feature identified in the $\theta_{Cs}=0.04$ ML spectrum presented in Fig. 1, although at this higher coverage the peak has shifted in energy towards E_F by an additional 0.2 eV.

When more Cs is deposited, the Cu image potential state continues to weaken, and becomes hard to distinguish from the background by a Cs coverage of 0.18 ML. In addition, the Cs-induced state continues to move towards the Fermi level and eventually becomes degenerate with the Cu bulk bands. As the saturation coverage at room temperature of 1 ML is approached, the energy of this feature remains approximately constant at about 0.3 eV above E_F. Another important aspect of the IPE spectra presented in Fig. 2 is the variation in the intensity of the Cs-induced spectral feature. Initially, as Cs coverage is increased, the feature strengthens and reaches a maximum intensity at $\theta_{Cs}=0.18$ ML. Further increase of the Cs coverage results in a decrease in the intensity of the adsorbate induced feature. At a Cs coverage of 0.29 ML, the peak has weakened to an extent that makes it difficult to distinguish from the background. However, as the alkali coverage is increased further, the Cs-derived state once again intensifies, as can be seen in the 0.39-ML spectrum, although it never reaches the intensity achieved at 0.18 ML. By $\theta_{Cs}=0.50$ ML, the intensity of the adsorbate state has decreased once more, only to reemerge at a coverage of 0.71 ML. A possible explanation for the intensity changes in the 0.29-ML coverage regime will be presented in Sec. V.

We point out that there appears to be some structure in the feature near E_F that changes as a function of coverage at low Cs exposures. This is clearly seen in Fig. 1, and for coverages less than 0.29 ML in the spectra of Fig. 2. As shall be seen, this enhanced emission at low alkali coverages is also evident on the Cu(111) substrate.

Figure 3 plots the energy and uncertainty in energy of the alkali-induced state as the Cs coverage is increased. Also plotted in the figure is the measured change in the work function of the Cs/Cu system as a function of Cs coverage. The work function versus coverage curve shows the well known rapid initial decrease of the work function as Cs is

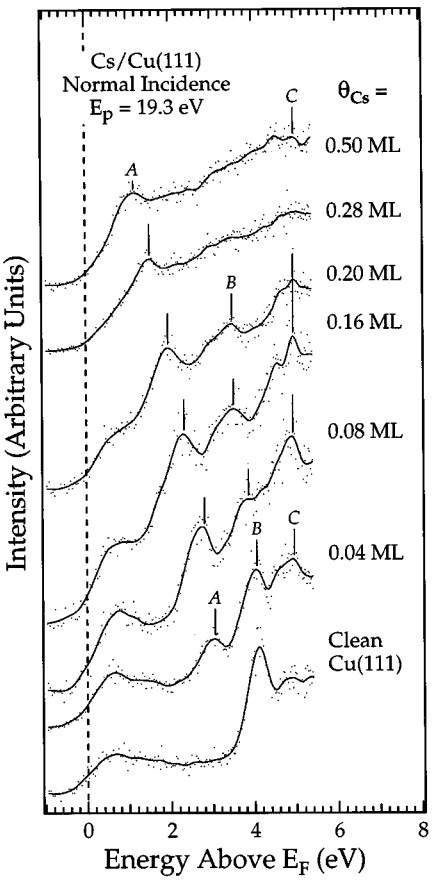

FIG. 4. Room-temperature, normal-incidence IPE spectra as a function of increasing Cs coverage on Cu(111) for an incident electron energy of 19.3 eV. The bottom spectrum is from clean Cu(111). The feature *A* is the Cs-induced state, while feature *B* is the image potential state of the Cs/Cu(111) system. The feature labeled *C* is associated with fluorescence from the Cs $5p_{1/2}$ level.

deposited onto the Cu sample, which reaches a minimum near 0.5 ML, followed by a small increase reaching a saturation value corresponding to metallic Cs as the coverage approaches 1 ML is reached. As mentioned above, the Cs-derived state shifts to lower energy above the Fermi level as the alkali coverage is increased. For the initial stages of adsorption this shift to lower energy closely follows the rapid decline of the work function of the Cs/Cu(100) system. Above $\theta_{Cs} \approx 0.5$ ML, however, the Cs state remains at an energy of ~ 0.3 eV above the Fermi level, and does not track the subsequent increase of the work function of the system.

The significant increases in the uncertainty of the Cs peak can largely be attributed to the pronounced decrease in intensity of the alkali peak. The first drop in intensity occurs at a relatively low alkali coverage (~ 0.29 ML) while the next one presents itself at about 0.5 ML, which is near the minimum of the Cs coverage vs work-function curve. We discuss a possible explanation for the first intensity decrease at $\theta_{Cs} \approx 0.29$ ML in Secs. VI and VII.

IV. Cs ON Cu(111)

In Fig. 4 we present normal-incidence IPE spectra acquired at room temperature for increasing Cs coverages on the Cu(111) substrate at a fixed incident energy of 19.3 eV.[40] Again, the bottom spectrum is from clean Cu(111). This spectrum is dominated by a single feature, the $n=1$ image potential state at ~ 4.1 eV above E_F.[41] In contrast to the clean Cu(100) spectrum, there is very weak emission below the image state because the Cu(111) surface has a projected bulk band gap extending from below the Fermi level to about 4.2 eV above E_F. The very small enhancement of emission at E_F due to the L-gap surface state of Cu(111), which is below E_F within ± 0.2 Å^{-1} of $\bar{\Gamma}$,[42] indicates the good angular resolution of our instrument.

As was the case with Cs on Cu(100), the IPE spectra are significantly modified by even small amounts of Cs on the sample. With only 0.04 ML of Cs on the sample, the intensity of the image potential state has decreased relative to the clean Cu surface, and the energy of the state has shifted to lower energy above E_F by about 0.2 eV. Moreover, a spectral feature, labeled *A* in Fig. 4, appears at ~ 3.0 eV above the Fermi level. This feature is distinct and well separated from the image potential state, and we thus attribute this peak to an adsorbate-induced level, most probably originating from the unoccupied Cs $5d$ level.

Even at the relatively low coverage of 0.04 ML of Cs, the adsorbate peak is quite intense. As additional Cs is deposited on the surface, the peak becomes more well defined and intense, and also moves toward the Fermi level. By a Cs coverage of 0.5 ML, the energy of the alkali feature has decreased to about 1.1 eV above E_F, which is essentially the same energy as the corresponding alkali feature on the $\theta_{Cs}=0.39$ ML spectrum from Cu(100). In contrast to the behavior of the Cs peak on Cu(100), the adsorbate state on the Cu(111) spectra remains well defined at all coverages that we explored. There is no evidence of the large modulations in the intensity of the feature and, although the intensity is largest at the relatively low coverage of 0.08 ML, the peak is always clearly distinguishable from the background.

A few additional features in the spectra presented in Fig. 4 require some comment. The first is the feature labeled *B* in the IPE spectra. This feature also decreases in energy as the Cs coverage is increased. Furthermore, the intensity of this peak decreases drastically as the Cs coverage nears the 0.5-ML regime. We believe that this feature is the remnant of the image potential state. Indeed, on both the Cu(100) and Cu(111) surfaces, the image potential state is essentially undetectable from the background for adsorbate coverages over ~ 0.2 ML. Another interesting feature in the spectra in Fig. 4 is the peak labeled *C*, which is visible at an energy of about 5.4 eV above E_F, corresponding to a fixed photon energy of 13.9 eV. This peak does not shift to lower energy as the alkali coverage is increased. Moreover, the peak is absent on the clean Cu(111) spectrum. As a result of these observations, we believe that this feature may be a fluorescence peak from the alkali overlayer, most likely originating from the excitation and subsequent decay of a core hole from the Cs $5p_{1/2}$ level by the incident electron beam.[43] Finally, as was the case on the Cu(100) substrate, the low-coverage ($\theta_{Cs}<0.2$ ML) spectra presented in Fig. 4 exhibit slightly enhanced emission just above E_F.

The momentum dependence of the Cs state along the $\langle 110 \rangle$ ($\bar{\Gamma}-\bar{M}$) direction of the SBZ is investigated in the series of spectra presented in Fig. 5. For these spectra, the Cs

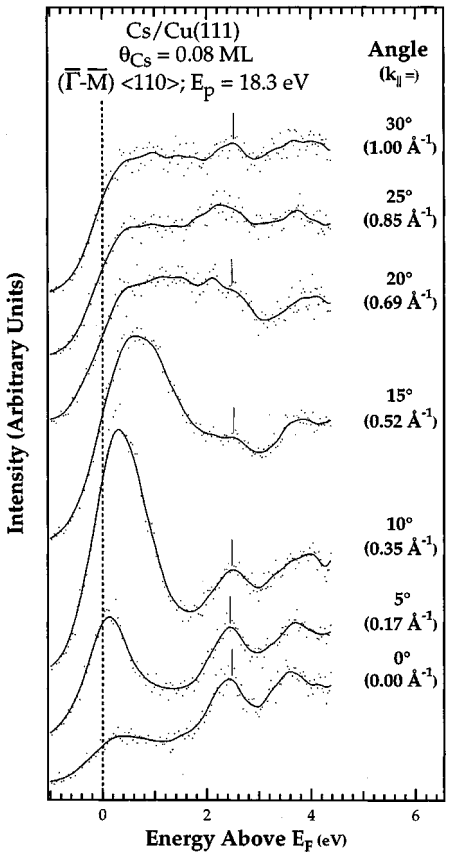

FIG. 5. IPE spectra of 0.08 ML of Cs on Cu(111) as a function of increasing angle for the incident electron beam along the $\langle 110 \rangle$ ($\overline{\Gamma}$-$\overline{M}$) direction. The excitation energy is 18.3 eV, and the substrate temperature was ~140 K during deposition and data acquisition. The bottom spectrum is from clean Cu(111). The quoted values of $k_{\parallel}$ are for the adsorbate feature identified by a vertical line at ~2.4 eV above E_F.

coverage was 0.08 ML, the substrate temperature was 140 K, and the incident electron energy was 18.3 eV. Away from $\overline{\Gamma}$, the spectra are dominated by the strong emission just above E_F, which originates primarily from direct transitions to a Cu bulk band that cross the Fermi level at $\theta = 10°$ as well as a Shockley-type surface state.[44] These features are not of primary interest here, and will not be discussed further. The normal-incidence spectrum at the bottom of Fig. 5 shows two features, a low-energy peak at about 2.4 eV above E_F, which we attribute to the Cs, and a higher-energy peak at 3.6 eV that we associate with the image potential state.

We now focus on the low-energy Cs-induced feature. In contrast to the image potential state, this feature does not disperse with $k_{\parallel}$ but rather remains at a constant energy of 2.4 eV. Such a lack of dispersion is expected for low Cs coverages, where the adsorbate has not formed an overlayer with long-range order.[45] At a $k_{\parallel}$ of $\sim 0.7\ \text{Å}^{-1}$, the alkali-induced state becomes degenerate with the Cu sp band. Under these conditions, the Cs feature appears less intense relative to the strongly emitting Cu bands. At a higher value of parallel momentum, the emission from the Cu bands is roughly constant across the spectrum, and the Cs feature is again clearly distinguishable at 2.4 eV.

In considering the results in Figs. 1, 2, and 5, we observe some striking similarities in the variations in intensity of the

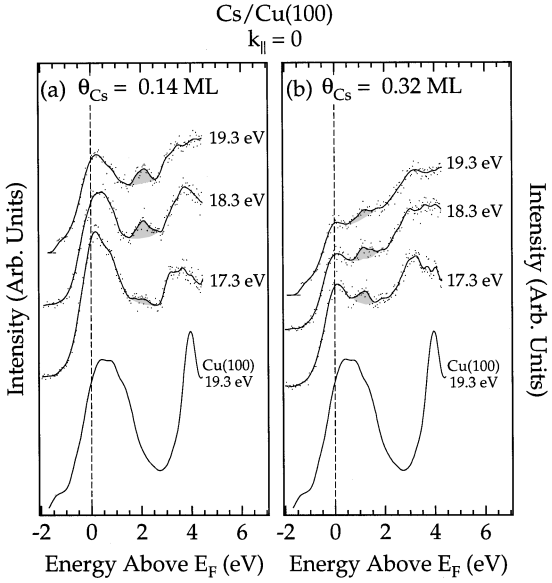

FIG. 6. Room-temperature, normal-incidence IPE spectra of the Cs/Cu(100) surface at different incident electron energies for (a) 0.14- and (b) 0.32-ML Cs coverages. In both panels the bottom spectrum is from clean Cu(100). The shaded areas highlight the Cs-derived feature.

Cs feature. On both substrates, the Cs feature was most intense and well defined when its energy and parallel momentum placed it in a projected bulk band gap of the substrate. When the feature was degenerate with the substrate bands, its intensity diminished significantly. This change in the apparent strength of the adsorbate feature is suggestive of an interesting momentum dependence to the adsorbate-substrate bond; we investigate this in more detail in Sec. V.

V. ENERGY-DEPENDENT SPECTRA OF Cs/Cu(100) AND Cs/Cu(111)

As noted in Sec. III the intensity of the Cs feature on the Cu(100) substrate exhibits a significant reduction at an alkali coverage near 0.29 ML, followed by an increase in intensity at 0.39 ML. To investigate this oscillatory intensity, we examined the IPE spectra of the Cs/Cu(100) system at coverages above and below 0.29 ML as a function of incident electron energies.[46] Figure 6(a) presents normal-incidence spectra of 0.14 ML of Cs on Cu(100) at several incident electron energies. For reference, a clean Cu(100) spectrum at an incident electron energy of 19.3 eV is also presented.

The 17.3 eV spectrum in Fig. 6(a) shows strong emission from the Cu sp bands from 0.0 eV to about 1.75 eV above E_F, as well as the weak remnant of the Cu image potential state at about 3.5 eV. An additional weak feature from the Cs overlayer is also visible in the Cu-projected bulk band gap at an energy of ~2.3 eV. As the incident electron energy is increased, the substrate sp bands decrease in intensity in a monotonic fashion, as does the image potential state. We attribute this reduction in the intensity to well-known matrix element effects for sp final states.[47] In contrast, the Cs feature intensifies as the incident electron energy is increased. This response is consistent with a d-like final state for the electron impinging on the surface, and we therefore conclude

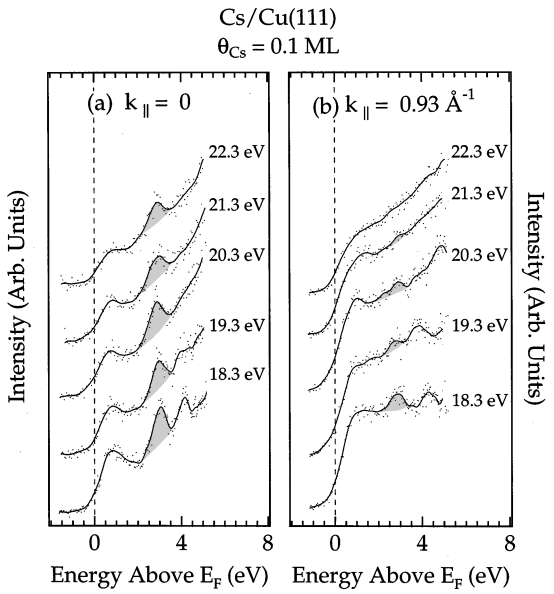

FIG. 7. Low-temperature ($\sim$140 K) IPE spectra from 0.1 ML of Cs on Cu(111) using different incident electron energies obtained at (a) normal incidence and (b) $k_{\|}$ of 0.93 Å^{-1} along the $\langle 110\rangle$ ($\overline{\Gamma}$-$\overline{M}$) direction. The shaded areas highlight the Cs-derived feature.

that the unoccupied Cs state contains a significant d-like component originating from the unoccupied Cs 5d level.[47]

A distinctly different picture emerges from the spectra in Fig. 6(b), which were acquired at normal incidence for an increased Cs coverage of 0.32 ML. While the emission from the Cu-projected bulk bands and the image state is clearly lower in these spectra due to the higher adsorbate coverage, their reduction in intensity with increasing electron energy is still apparent. However, the Cs feature, which has moved to an energy of $\sim$1.3 eV, now *decreases* in intensity as the excitation energy is increased. As the substrate sp levels and the Cs feature exhibit the same response to increasing excitation energy, we conclude that the Cs-induced state now has a dominant sp-like orbital character.

We performed similar measurements of energy-dependent IPE spectra of Cs on the Cu(111) substrate. However, motivated by the results presented in Fig. 5, we acquired spectra of a fixed Cs coverage of 0.1 ML at both normal incidence and at a constant $k_{\|}$ of 0.93 Å^{-1} along the $\langle 110\rangle$ ($\overline{\Gamma}$-$\overline{M}$) direction of the SBZ. The normal-incidence spectra are presented in Fig. 7(a), where the adsorbate-induced state is plainly evident at about 2.5 eV above E_F; the sharp feature at $\sim$3.6 eV is the image potential state. In this instance, the presence of the Cu emission near E_F proves beneficial, as it shows a characteristic decrease in intensity with increasing excitation energy. A similar decrease in intensity is evident in the image potential state. The intensity of the Cs-induced state, on the other hand, remains nearly constant, and thus we believe that our assignment of the unoccupied Cs 5d level to this feature is consistent with the spectra in Fig. 7(a).

Figure 7(b) presents IPE spectra for the same system at increasing excitation energies acquired at a constant $k_{\|}$ of 0.93 Å^{-1}. In this set of data, the Cs-derived state is degenerate with the unoccupied portion of the Cu sp band. These spectra show that the Cs-derived state now decreases in intensity with increasing incident electron energy, which is characteristic of sp-like orbital character. We discuss the implications and examine possible explanations for this behavior in Sec. VI.

VI. DISCUSSION

The very low-coverage data for Cs on Cu(100) in Fig. 1, and the lowest coverage data for Cs on Cu(111) presented in Fig. 4, indicate that a Cs-derived feature originates at about 2.9 eV above the Fermi level in the zero-coverage limit. The Cs feature shifts to lower energy above E_F as the alkali coverage is increased. A similar pattern of an initial decrease in the energy of unoccupied alkali-induced levels, followed by a leveling off in the energy position as room-temperature saturation coverage is approached, has been reported for K and Cs on Al(111),[13] Na/Ni(111),[26] Na/Cu(110),[25] and K/Ag(110).[27] This decrease in the energy of the adsorbate level is thought to be due to the strengthening dipole potential on the surface as the alkali coverage is increased.[3,48] This interpretation only applies to the initial stages of deposition; at higher coverages, the wave function overlap of the adsorbate's orbitals is considerable, leading to a reduction of the dipole field[49] and a leveling off in the energy of the adsorbate states.

All the normal incidence spectra presented exhibit enhanced emission near E_F at low Cs coverages [cf. Figs. 1, 2, and 6(a) for Cu(100), and Figs. 4, 5, and 7(a) for Cu(111)]. Furthermore, as can be seen in Figs. 6 and 7, the intensity just above E_F on both substrates decreases with incident electron energy, which indicates that this enhanced emission is primarily of sp-orbital character.[47] We believe that this additional emission may originate from the unoccupied tail of the Cs 6s resonance, as was reported for Cs on Al(111).[13]

The lack of dispersion with $k_{\|}$ that is evident in the data presented in Fig. 5 is also not unusual as the alkali coverage is very low, and the adsorbate has not formed an ordered overlayer. However, there does appear to be some momentum dependence to the adsorbate-derived features even at these low coverages, as shall be addressed shortly.

The interpretation of the intensity variations that are apparent in the fixed incident electron energy spectra for Cs/Cu(100) and Cs/Cu(111) warrants further discussion. The behavior of the adsorbate level at $\overline{\Gamma}$ for the two surfaces is very different. Figure 2 shows that at moderate coverages on Cu(100) ($\theta_{Cs}\sim$0.18 ML), the Cs state is clear and well defined. As the Cs coverage increases the adsorbate level first weakens ($\theta_{Cs}\sim$0.29 ML), only to reemerge as a distinct level at higher coverages ($\theta_{Cs}\sim$0.39 ML). The picture is very different for Cu(111) at $\overline{\Gamma}$ (cf. Fig. 4). On that surface, the alkali feature remains distinct and well defined at all coverages which we explored. However, for a fixed coverage (cf. Fig. 5), the Cs feature on the Cu(111) surface showed intensity variations as a function of parallel momentum similar to those exhibited by Cs on Cu(100) as a function of Cs coverage.

The energy-dependent spectra presented in Figs. 6 and 7 offer some guidance in the interpretation of these observations. The spectra showed that the apparent orbital character of the Cs feature changed from sp-like to d-like for both the Cu(100) and Cu(111) substrates. Furthermore, this change in orbital character was achieved by varying very dissimilar

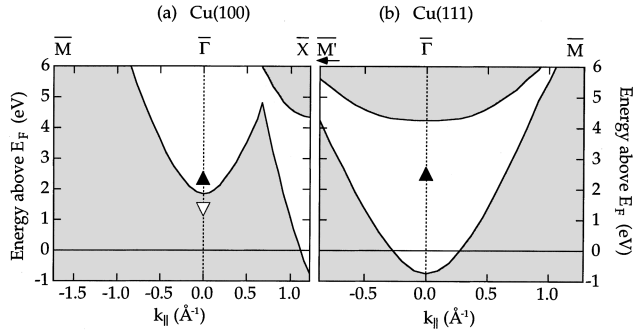

FIG. 8. The band structure of Cu projected onto the (a) (100) and (b) (111) surfaces. The shaded areas indicate projected bulk bands, while unshaded areas are projected band gaps. The triangles mark the positions of Cs-induced features in the IPE spectra of Figs. 6 and 7; filled triangles indicate d-like orbital character, and the unfilled triangles denote sp-like orbital character.

experimental parameters: increasing the Cs coverage in the case of Cu(100) versus changing the parallel momentum for the Cu(111) substrate. The mechanism responsible for the change in the orbital character of the alkali state is therefore not immediately apparent. However, a common factor emerges upon inspection of the electronic band structure of the two substrates.

The projected band structures for the two substrates are plotted in Fig. 8(a) for Cu(100) and Fig. 8(b) for Cu(111).[50] The unshaded areas indicate the presence of a projected bulk band gap, while the shaded portions show the regions of energy and parallel momentum spanned by the bulk direct transitions. We also indicate the locations of the Cs peaks from Figs. 6 and 7 along with symbols which denote the predominant orbital character for the Cs-derived spectral features. As can be seen, two of the adsorbate-induced features lie within a projected bulk band gap of the substrate, the lower-coverage Cs state at about 2.3 eV on the Cu(100) surface [Fig. 8(a)], and the state at $\bar{\Gamma}$ for the Cu(111) substrate [Fig. 8(b)]. Both these states have a predominantly d-like orbital character. Conversely, the adsorbate features which are degenerate with the substrate projected bulk band gaps, the 0.32-ML state on the Cu(100) substrate and the feature at a $k_{\parallel}$ of 0.93 Å^{-1} on Cu(111), appear to have a mostly sp-like orbital character. Thus, the orbital character of the Cs feature is correlated with degeneracy with the substrate bands; the Cs feature exhibits d-like orbital character when it is in a projected bulk band gap, and sp-like orbital character when it is degenerate with the substrate sp bands. Furthermore, this effect is apparent whether degeneracy with the substrate bands is achieved by varying coverage to modify the energy of the Cs feature, as was the case with the Cu(100) data, or by accessing a different part of the SBZ, as was done with the Cu(111) substrate.

Momentum-dependent modifications of adsorbate energy levels are typically associated with dispersion of *energy* with $k_{\parallel}$, a phenomenon which is restricted to ordered overlayers. We believe this is the first report of a momentum dependence to the *orbital character* of an adsorbate spectral feature, and our results may indicate a significant amount of hybridization of the alkali adsorbate/metal substrate bond.

The behavior of the alkali-induced levels in our data shows some similarities to a calculation by Liebsch of the electronic structure of the $c(2\times2)$O/Ni(100) system.[51] By comparing this system to an unsupported ordered O layer with the same O-O separation, Liebsch shows that, due to the hybridization of the adsorbate-substrate bands, the energy width of the adsorbate bands can be modified. The overlayer bands develop a resonance width in those regions of the SBZ where substrate bands of a compatible symmetry are present. A similar effect develops in the density of states of the substrate, which is enhanced when adsorbate levels of appropriate symmetry are accessible. These effects were later verified in an angle-resolved valence-band photoemission study of the $c(2\times2)$S/Fe(100) system,[52] where the authors report that the S p bands were broader in those regions of the SBZ where substrate bands are present in comparison to regions of the SBZ where there is a substrate projected bulk band gap.

We believe our IPE results for Cs/Cu(100) and Cs/Cu(111) may similarly indicate a hybridization of the overlayer-substrate bonds which result in some dependence on parallel momentum. For low coverages at $\bar{\Gamma}$ on both copper surfaces, the Cs state develops in the projected bulk band gap of Cu. Thus the Cs levels cannot access the substrate levels and the adsorbate state exhibits its intrinsic d character. However, in regions of the SBZ where the local density of states of the substrate sp levels is significant, the d-like component of the adsorbate is undetectable due to the large resonance width and the dominant contribution to the IPE spectra is the substrate sp levels. This effect is independent of the mechanism used to access different parts of the substrate's band structure, e.g., lowering the energy of the adsorbate level via increased coverage or varying the $k_{\parallel}$ of the incident electrons.

One difficulty with this interpretation is that our observations of these momentum-dependent spectral features occur for low alkali coverages where long-range order of the overlayers is not observed. Indeed, as is evident in Fig. 5, the Cs feature did not disperse with $k_{\parallel}$ for the Cs/Cu(111) system. However, LEED studies indicate that at reduced temperatures (<50 K) on the Cu(111) surface, Cs tends to form a hexatic liquid phase for coverages as low as 0.1 ML.[53] These structural studies, coupled with our observation of a momentum dependence of certain adsorbate states, suggests the presence of sufficient short-range order on the surfaces to affect bonding, but not enough long-range order to produce an observable, distinct LEED pattern.

VII. SUMMARY AND CONCLUSIONS

In summary, we performed a series of IPE experiments of Cs on the Cu(100) and Cu(111) substrates. On both surfaces at normal incidence, the adsorbate level develops in the substrate projected bulk band gap at about 2.9 eV above E_F. With increasing alkali coverage, this feature moves towards E_F. This observation is consistent with results from other IPE investigations of alkalis on metals, and can be understood in terms of a strengthening dipole field as the alkali coverage increases. At $\theta_{\text{Cs}}\sim0.08$ ML, the Cs-derived feature on Cu(111) exhibits no dispersion with $k_{\parallel}$, which is consistent with an absence of long-range order at low adsorbate coverages.

Large variations in the intensity of the Cs-induced feature

are correlated with changes in the orbital character of the adsorbate level, as identified in energy-dependent IPE spectra. Both of these effects can be interpreted as evidence for hybridization of the adsorbate/substrate bond. The adsorbate's orbital character is evident when the adsorbate level lies in a projected bulk band gap of the substrate, while the substrate's orbital character becomes dominant when the adsorbate level is degenerate with the projected bulk bands of the substrate. These results are consistent with a theoretical treatment of the $c(2\times2)$O/Ni(100) system and an angle-resolved photoemission study of $c(2\times2)$S/Fe(100).

ACKNOWLEDGMENTS

This study was financially supported by the National Science Foundation under Grant No. NSF-DMR 94-11610. In addition, this material is based upon work done by D.A.A., who was supported by the National Science Foundation.

*Author to whom correspondence should be addressed.

[1] *Physics and Chemistry of Alkali Adsorption*, edited by H. P. Bonzel, A. M. Bradshaw, and G. Ertl (Elsevier, Amsterdam, 1989).
[2] H. Ishida, Phys. Rev. B **38**, 8006 (1988).
[3] B. N. J. Persson and H. Ishida, Phys. Rev. B **42**, 3171 (1990).
[4] H. Ishida, Phys. Rev. B **42**, 10 899 (1990).
[5] G. Pacchioni and P. S. Bagus, Surf. Sci. **286**, 317 (1993).
[6] J. Neugerbauer and M. Scheffler, Surf. Sci. **287/288**, 572 (1993).
[7] B. Wenzien, J. Bromet, J. Neugerbauer, and M. Scheffler, Surf. Sci. **287/288**, 559 (1993).
[8] C. Stampfl, J. Burchhardt, M. Nielsen, D. L. Adams, M. Scheffler, H. Over, and W. Moritz, Surf. Sci. **287/288**, 418 (1993).
[9] J. Neugerbauer and M. Scheffler, Phys. Rev. B **46**, 16 067 (1992).
[10] For an exhaustive review, see R. D. Diehl and R. McGrath, Surf. Sci. Rep. **23**, 49 (1996).
[11] R. Dudde and B. Rheil, Surf. Sci. **287/288**, 614 (1993).
[12] N. Fischer, S. Schuppler, R. Fischer, T. Fauster, and W. Steinmann, Phys. Rev. B **43**, 14 722 (1991).
[13] K. H. Frank, H. J. Sanger, and D. Heskett, Phys. Rev. B **40**, 2767 (1989).
[14] H. Ishida, Phys. Rev. B **40**, 1341 (1989).
[15] E. Wimmer, A. J. Freeman, J. R. Hiskes, and A. M. Karo, Phys. Rev. B **28**, 3074 (1983).
[16] E. Wimmer, J. Phys. F **13**, 2313 (1983).
[17] C. A. Papageorpoulos, Phys. Rev. B **25**, 3740 (1982).
[18] D. A. Papaconstantopoulos, *Handbook of the Band Structure of Elemental Solids* (Plenum, New York, 1986).
[19] R. Dudde, K. H. Frank, and B. Rheil, Phys. Rev. B **41**, 4897 (1990).
[20] R. Dudde, L. S. O. Johansson, and B. Rheil, Phys. Rev. B **44**, 1198 (1991).
[21] N. Memmel, G. Rangelov, E. Bertel, and V. Dose, Phys. Rev. B **43**, 6938 (1991).
[22] N. Memmel, G. Rangelov, and E. Bertel, Surf. Sci. **285**, 109 (1993).
[23] D. Heskett, K. H. Frank, E. E. Koch, and H. J. Freund, Phys. Rev. B **36**, 1276 (1987).
[24] C. Su, D. Tang, and D. Heskett, Surf. Sci. **310**, 45 (1994).
[25] D. Tang, C. Su, and D. Heskett, Surf. Sci. **295**, 427 (1993).
[26] D. Tang and D. Heskett, Phys. Rev. B **47**, 10 695 (1993).
[27] W. Jacob, E. Bertel, and V. Dose, Phys. Rev. B **35**, 5910 (1987).
[28] D. P. Woodruff and N. V. Smith, Phys. Rev. B **41**, 8150 (1990).
[29] F. G. Curti, D. A. Arena, and R. A. Bartynski (unpublished).
[30] N. G. Stoffel and P. D. Johnson, Nucl. Instrum. Methods Phys. Res. A **234**, 230 (1984).
[31] C. Lang, T. Mandel, C. Laubschat, and G. Kaindl, J. Electron Spectrosc. Relat. Phenom. **52**, 49 (1990).
[32] J. Cousty, R. Riwan, and P. Soukiassian, Surf. Sci. **151/153**, 297 (1985).
[33] S. Å. Lindgren, L. Walldén, J. Rundgren, P. Westrin, and J. Neve, Phys. Rev. B **28**, 6707 (1983).
[34] J. A. Knapp, F. J. Himpsel, and D. E. Eastman, Phys. Rev. B **19**, 4952 (1979).
[35] D. P. Woodruff, N. V. Smith, P. D. Johnson, and W. A. Royer, Phys. Rev. B **26**, 2943 (1982).
[36] D. P. Woodruff, S. L. Hulbert, P. D. Johnson, and N. V. Smith, Phys. Rev. B **31**, 4046 (1985).
[37] F. J. Himpsel and J. E. Ortega, Phys. Rev. B **46**, 9719 (1992).
[38] P. D. Johnson and N. V. Smith, Phys. Rev. B **27**, 2527 (1983).
[39] V. Dose, W. Altmann, A. Goldmann, U. Kolac, and J. Rogozik, Phys. Rev. Lett. **52**, 1919 (1984).
[40] The energy values quoted in the discussion of Fig. 4 should be used with caution due to difficulties with the energy calibration of the instrument. However, none of the basic conclusions in this section are affected by the absolute energy calibration of the IPE spectrometer.
[41] S. L. Hulbert, P. D. Johnson, N. G. Stoffel, W. A. Royer, and N. V. Smith, Phys. Rev. B **31**, 6815 (1985).
[42] S. D. Kevan, Phys. Rev. Lett. **50**, 526 (1983).
[43] K. Tsuei and P. D. Johnson, Phys. Rev. Lett. **71**, 1099 (1993).
[44] W. Jacob, V. Dose, U. Kolac, T. Fauster, and A. Goldmann, Z. Phys. B **63**, 459 (1986).
[45] W. C. Fan and A. Ignatiev, Phys. Rev. B **37**, 5274 (1988).
[46] A preliminary description of these results was presented in D. A. Arena, F. G. Curti, and R. A. Bartynski, Surf. Sci. **369**, L117 (1996).
[47] J. E. Ortega and F. J. Himpsel, Phys. Rev. B **47**, 16 441 (1993).
[48] E. Bertel, Appl. Phys. A: Solids Surf. **53**, 356 (1991).
[49] H. Ishida and K. Terakura, Phys. Rev. B **36**, 4510 (1987).
[50] Calculated using a combined interpolation scheme provided by N. V. Smith and L. F. Matheiss, Phys. Rev. B **9**, 1341 (1974); N. V. Smith, *ibid.* **19**, 5019 (1979).
[51] A. Leibsch, Phys. Rev. B **17**, 1653 (1978).
[52] R. A. Didio, E. W. Plummer, and W. R. Graham, Phys. Rev. Lett. **52**, 693 (1984).
[53] W. C. Fan and A. Ignatiev, J. Vac. Sci. Technol. A **6**, 735 (1988).